Mechanical behavior of Cu–Zr bulk metallic glasses (BMGs): A molecular dynamics approach*

Muhammad Imran[a)†], Fayyaz Hussain[a)b)], Muhammad Rashid[a)], Yongqing Cai[b)], and S. A. Ahmad[a)]

[a)] *Department of Physics Simulation Lab, The Islamia University of Bahawalpur* 63100, *Pakistan*
[b)] *Department of Physics, National University of Singapore*, 2 *Science Drive* 3, 117542, *Singapore*

(Received 26 December 2012; revised manuscript received 27 March 2013)

In the present work, three-dimensional molecular dynamics simulation is carried out to elucidate the nanoindentation behaviors of CuZr Bulk metallic glasses (BMGs). The substrate indenter system is modeled using hybrid interatomic potentials including both many-body Finnis Sinclair (FS) and two-body Morse potentials. A spherical rigid indenter (diameter = 60 Å(1 Å = 10^{-10} m)) is employed to simulate the indentation process. Three samples of BMGs including $Cu_{25}Zr_{75}$, $Cu_{50}Zr_{50}$, and $Cu_{75}Zr_{25}$ are designed and the metallic glasses are formed by rapid cooling from the melt state at about 2000 K. The radial distribution functions are analyzed to reveal the dynamical evolution of the structure of the atoms with different compositions and different cooling rates. The mechanical behavior can be well understood in terms of load-depth curves and Hardness-depth curves during the nanoindentation process. Our results indicate a positive linear relationship between the hardness and the Cu concentration of the BMG sample. To reveal the importance of cooling rate provided during the processing of BMGs, we investigate the indentation behaviors of $Cu_{50}Zr_{50}$ at three different quenching rates. Nanoindentation results and radial distribution function (RDF) curves at room temperature indicate that a sample can be made harder and more stable by slowing down the quenching rate.

Keywords: Bulk metallic glasses (BMGs), nanoindentation, deformation, quenching rate

PACS: 62.20.F–, 62.20.mm, 62.20.mt **DOI:** 10.1088/1674-1056/22/9/096101

1. Introduction

Bulk metallic glasses (BMGs) have attracted much attention in recent years due to their potential applications in industry.[1] BMGs exhibit excellent surface finish, are easy to process, have high mechanical strength, and minimal shrinkage. BMGs are among the promising candidate materials for the fabrication of micro-electro-mechanical systems (MEMS), especially three-dimensional structures.[2–4] These advantages of BMGs as structural materials have opened new application fields; thus, the mechanical behaviors of BMGs have again become a matter of great interest. Mechanical behaviors of metallic glasses show various features that are significantly different from those of crystalline alloys, ceramic crystals, and other glass.[5–7] BMGs as structural materials could revolutionize the relevant fields due to their promising mechanical behavior from a combination of their excellent strength, toughness, elastic limit, corrosion resistance, and wear resistance. These superior properties have made them versatile engineering materials for many scientific technological commercial applications.[8–12]

In recent years, immense work has been reported on the mechanical and structural properties of BMGs. The structure and property relationship of BMG has aroused great interest, particularly in CuZr binary system. CuZr binary systems are widely regarded as a promising candidate for BMGs. A clear correlation between glass forming ability and the density changes is reported in CuZr BMGs.[13] Structural stability and thermal stability are observed in a wide compositional range of CuZr BMGs using X-ray diffraction and the pair distribution function. Results showed monotonic changes for different compositions.[14,15] The high energy X-ray synchrotron diffraction technique has been used to investigate the behaviors of $Zr_{50}Cu_{50}$ and $Zr_{35}Cu_{65}$ BMGs under uniaxial tensile loading. Their results show that the elastic deformations are present, owing to bond reorientation and changes in chemical short range ordering.[16] An X-ray adsorption fine structure method was used to study the local atomic structures of CuZu BMGs.[17] BMGs with amorphous structuress have no clear deformation mechanism which can be accommodated in terms of shear bands.[18,19]

Among the methods utilized in nanotechnology, a versatile and widely used tool for inspecting mechanical behavior, such as the elastic constant, hardness, and transition from the elastic-to-plastic region of the material, is nanoindentation.[20–22] Recently, it has been proved to be a popular technique for investigating mechanical characteristics of BMGs. Nonoindentation is also proved to be very useful for investigating the mechanical behaviors of very small volumes of materials including BMGs.[23–26] Indentation has been used to investigate incipient plasticity and shear band forma-

*Project supported by the Higher Education Commission (HEC) of Pakistan (Grant No. +923445490402).
†Corresponding author. E-mail: anam_iub@yahoo.com

tion in BMG. The deformation results at higher load provide evidence about the structural change which can be related to possible free volume expansion.[27] Nanoindentation with a spherical indenter was used to analyze the perfect elastic-to-plastic deformation transition in BMG which showed a clear popin event on the load-displacement plot.[28] Instrumented nanoindentation over a broad range of loading rates was performed to study the plastic deformation of Zr based BMGs; this work revealed that the plastic flow exhibited conspicuous serrations at low loading rates, which is less prominent at higher indentation rates.[29] Molecular dynamics simulations of Cu_x Zr_{100-x} reveal that a Cu-centered small icosa-hedral cluster (ICO) is a basic structured object present in the systems, while an increase in Cu concentration causes an increase in their number.[30]

A binary $Cu_{49.3}Zr_{50.7}$ grown on Si (1 1 0) is subjected to nanoindentation to investigate the mechanical behavior of the BMG film which indicates that unlike other BMG this composition does not show an indentation size effect (ISE).[31] Nanoindentation of ion irradiated Zr based BMG showed that the load-depth curve possesses a transition from serrated to continuous flow with ion irradiation damage increasing.[32] Short range ordering has been observed in the atomic structures of $Cu_{35}Zr_{65}$, $Cu_{50}Zr_{50}$, and $Cu_{65}Zr_{35}$, and BMGs were observed using various diffraction techniques.[15] Time dependent deformation was analyzed in binary Cu–Zr BMGs in a nanoindentation creep experiment, which revealed a pronounced creep behavior for the as-cast sample as compared with the annealed sample.[33] Investigation of inhomogeneous BMG structures showed a remarkable increase in the onset slope of load-displacement curve by increasing the diameter of glass rod and annealing temperature.[34]

Molecular dynamics (MD) simulation has been widely used to simulate nanoindentation problems. Many studies have been carried out to characterize the atomic structures and mechanical properties of CuZr BMGs using MD simulations. For instance, MD simulation was performed to investigate the effect of pores on the mechanical behavior of porous $Cu_{46}Zr_{54}$ during nanoindentation, which showed that the presence of pores is conducible to the initiation of shear bands and causes strain concentration.[35] Metallic glass thin films were subjected to nanoindentation, and MD simulation was used to observe their strain localizations and plastic deformations.[36] Results revealed that the most constrained samples exhibit the highest hardness. MD study with embedded atom method (EAM) was conducted to determine the effect of cyclic loading on the overall strength and plasticity of $Cu_{63.5}Zr_{36.5}$metallic glass.[37] Simulations were carried out on $Cu_{0.50}Zr_{0.50}$ and $Mg_{0.85}Cu_{0.15}$ metallic glasses to study the formations of shear bands during the indentation process. Results indicate that loading rate, indenter size and cooling rate are important factors that may affect the process.[38] To understand how the stress field and material structure interact to control the deformation process beneath the indenter, MD simulation was employed.[39] MD studies also revealed that the extensive strength of BMG arises from the percolating backbone of short-range ordering.[40]

In this work, we aim to characterize the mechanical behaviors using nanoindentation for a wide compositional range of Cu–Zr BMGs including $Cu_{25}Zr_{75}$, $Cu_{50}Zr_{50}$, and $Cu_{75}Zr_{25}$. To investigate the effect of Zr percentage within the bulk metallic glass on the mechanical behavior, the load-depth and hardnessdepth curves for all compositions are compared. Secondly, $Cu_{50}Zr_{50}$ BMG is chosen to investigate the effect of cooling rate on the mechanical behavior of BMG. For this purpose, the $Cu_{50}Zr_{50}$ system is cooled rapidly at three different cooling rates and finally the load-depth and radial distribution function (RDF) curves are compared.

2. Structural model and sample preparation

The configuration of the simulated indenter and substrate is shown in Fig. 1. The substrate material consists of three different compositions of Cu and Zr, i.e., $Cu_{25}Zr_{75}$, $Cu_{50}Zr_{50}$, and $Cu_{75}Zr_{25}$. The substrate sizes are 100 Å × 100 Å × 60 Å along (1 1 −2), (1 −1 0), and (1 1 1) directions respectively, containing 41526 atoms. A spherical rigid Cu indenter (diameter = 60 Å) with (1 0 0) tip toward the substrate is used for the indentation process. In order to analyze the effect of cooling rate on the mechanical behavior, the $Cu_{50}Zr_{50}$ configuration is selected and subjected to three different cooling rates. The size and orientation of the simulation cell are kept the same as those described earlier.

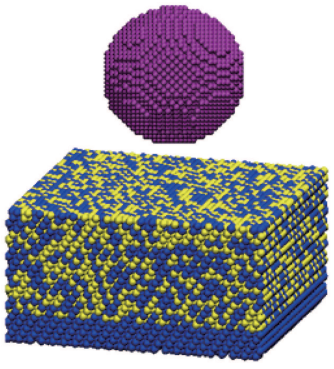

Fig. 1. (color online) A typical simulation cell ($Cu_{50}Zr_{50}$) used for the present work, where blue represents Cu atoms, yellow refers to Zr atoms and purple indicates the atoms of rigid a spherical Cu indenter.

3. Computational details and interatomic potential

Our computational cell consists of three types of atoms, Cu and Zr atoms in the substrate, and Cu atoms in a rigid Cu indenter. The choice of these potentials is supported by previous simulations performed for the nanoindentation. There

are five types of interactions possibly occurring between these atoms. The interactions between Cu(substrate)–Cu(substrate), Zr–Zr, and Cu(substrate)–Zr pairs are dealt with using a well-known generalized form of EAM potentials developed by Finnis and Sinclair.[41] The total energy E_i of an atom i is given by

$$E_i = F_\alpha \left(\sum_{j \neq i} \rho_{\alpha\beta}(r_{ij}) \right) = \frac{1}{2} \sum_{j \neq i} \phi_{\alpha\beta}(r_{ij}),$$

where F is the embedding energy which is a function of atomic electron density ρ, ϕ is a pair potential interaction, and α and β are the element types of atoms i and j.

The interaction between Cu (substrate)–Cu (indenter) and Zr–Cu (indenter) pairs is provided by two-body Morse interatomic potential, and the Morse potential energy, $U_{\text{Morse}}(r_{ij})$, can be described with three parameters as

$$U_{\text{Morse}}(r_{ij}) = D \left[\mathrm{e}^{-2\alpha(r_{ij}-r_0)} - 2\,\mathrm{e}^{-\alpha(r_{ij}-r_0)} \right]_{r_{ij}<r_c}$$

where D is the cohesion energy of exchange interaction, r_0 is the equilibrium distance, and r_{ij} is the separation distance between atoms i and j. The α is fitted to the bulk modulus of the material. For a Cu (substrate)–Cu (indenter) pair the parameters of Morse interatomic potential D, α and r_0 are 0.4332 eV, 1.6456 Å^{-1} and 2.7629 Å, respectively; for Zr–Cu (indenter) pair the parameters of Morse interatomic potential D, α and r_0 are 0.6032 eV, 1.5233 Å^{-1}, and 3.1315 Å, respectively. In addition, Morse potentials are selected because they are simple, computationally inexpensive, and have been used in several studies to control the interaction between the indenter and the substrate. Whereas Cu (indenter)–Cu (indenter) atoms of the indenter are all taken to be rigid and treated as a single particle. Hence, no description is required for the interaction.

4. Simulation process

A large-scale atomic/molecular massively parallel simulator (LAMMPS)[42] is used to perform the simulation throughout this work. To obtain the glassy structure, the substrate is subjected to periodic boundary conditions in all three dimensions. The substrate is first equilibrated at 2000 K and then quenched at a cooling rate of 2 K/ps down to 300 K in temperature steps of 200 K. After each temperature step, the substrate is allowed to equilibrate at that temperature for 200 ps. Finally, the substrate equilibrates at 300 K for 500 ps. In the indentation process, the bottom five layers of the substrate are kept fixed, periodic boundary conditions are used along the sides of the substrate whereas the upper part is subjected to a free boundary condition. A rigid Cu indenter sphere is placed 3 Å above the top surface of the substrate. The force acting on an individual particle of an indenter is calculated by summing the force contributions from the surrounding atoms. Time step for the whole simulation process is 1 fs. The projected contact area is calculated using the following formula:

$$A = \pi R d,$$

where R and d are the radius of indenter sphere and the indentation depth respectively. Hardness is calculated using the following relation:

$$H = \frac{F_{\max}}{A_{\mathrm{c}}},$$

where $F_{\max}$ and A_{c} are the maximum indentation load and the projected contact area, respectively.

5. Results and discussion

5.1. Effect of component concentration (in %) in BMG

To investigate the effect of component concentration (in %) on the mechanical behavior of binary BMG, we choose three different Cu and Zr compositions, i.e., $Cu_{25}Zr_{75}$, $Cu_{50}Zr_{50}$, and $Cu_{75}Zr_{25}$. The sample substrates are first heated and then equilibrated at 2000 K for 500 ps. Then the quenching start at a cooling rate of 2 K/ps down to 300 K in temperature steps of 200 K followed by equilibration after each temperature step. Finally, all the sample substrates are equilibrated at 300 K for 500 ps. The final processed samples are shown in Fig. 2.

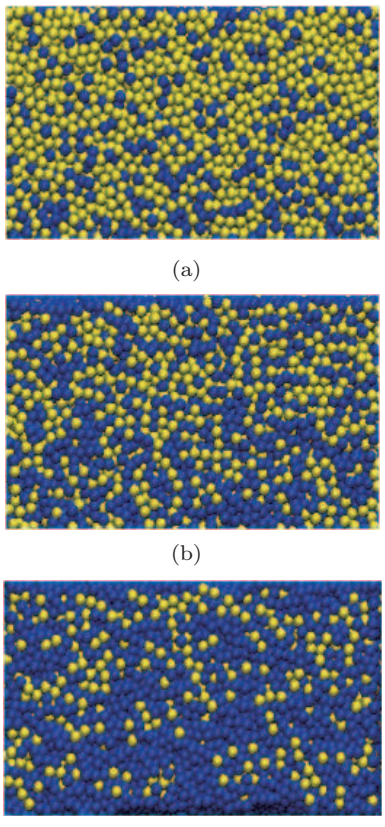

Fig. 2. (color online) Final amorphous structures for $Cu_{25}Zr_{75}$ (a), $Cu_{50}Zr_{50}$ (b), and $Cu_{75}Zr_{25}$(c), where yellow and blue colors represent Zr and Cu atoms respectively.

In order to investigate the effect of component concentration on the mechanical behavior, each sample substrate is subjected to nanoindentation using spherical rigid Cu indenter, with the substrate indented at a constant velocity. The obtained load-depth curves for all configurations are compared as shown in Fig. 3.

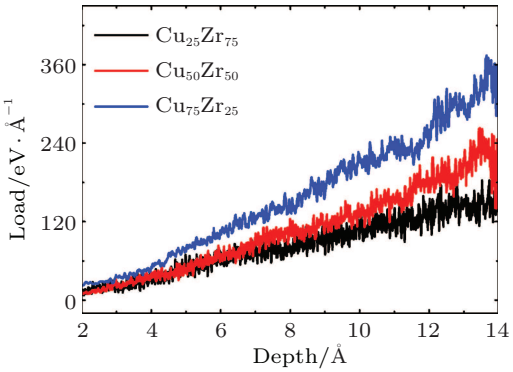

Fig. 3. (color online) Plots of load versus depth, showing the effects of various Cu and Zr concentrations.

It can be clearly observed from load-depth curves for different Zr concentrations in the three samples that mechanical behaviors change considerably with the variation of Zr concentration. The value of the load is highest for $Cu_{75}Zr_{25}$ (minimum Zr concentration) and lowest for $Cu_{25}Zr_{75}$ (maximum Zr concentration). Hence, samples with a smaller concentration of Zr are more difficult to indent. The load-hardness curves for the indentation process are shown in Fig. 4.

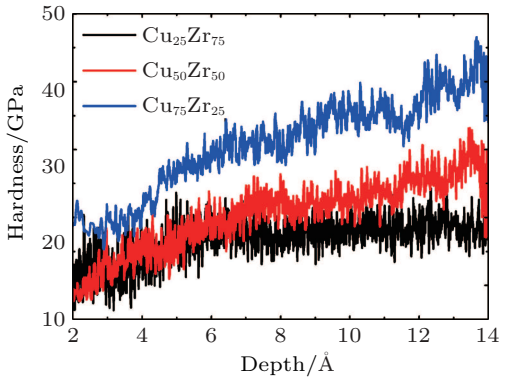

Fig. 4. (color online) Plots of hardness versus depth, showing the effects of different Cu and Zr concentrations.

It can be seen from the hardness-depth curves for different concentration BMGs that $Cu_{75}Zr_{25}$ is hardest in the three samples and $Cu_{25}Zr_{75}$ shows the least hardness, whereas $Cu_{50}Zr_{50}$ shows its mechanical hardness falling in between. This difference in mechanical behavior may be related to the difference in structure among the three samples. To analyze the possible structural differences for different compositions, the radial distribution function (RDF) curves for all configurations are compared as shown in Fig. 5.

Of the first peaks of RDF, the first peak for $Cu_{25}Zr_{75}$ is biggest and that for $Cu_{75}Zr_{25}$ is smallest, implying that the structural stability increases with copper concentration in the sample increasing. The first peak of the RDF indicates the average distance at which we find the nearest neighboring atom $g_{Cu-Zr}(r)$ i.e., between the unlike atoms. It can be noted that the sample with the highest peak has a less stable structure and hence exhibits the least hardness and vice versa. These results are also similar to the earlier experimental results.[31]

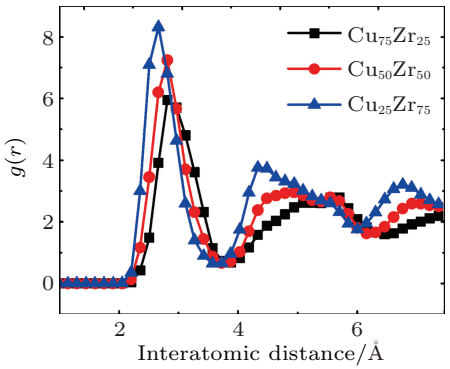

Fig. 5. (color online) Plots of RDF versus interatomic distance, showing the effect of different Cu and Zr concentrations.

5.2. Effect of cooling rate on mechanical behavior

To reveal the influence of cooling rate on mechanical behavior we choose $Cu_{50}Zr_{50}$ as BMGs. The samples are first heated to 2000 K and then cooled down to 300 K via three different cooling rates (i.e., 1.33 K/ps, 2 K/ps, and 4 K/ps). Finally, all the samples are maintained at room temperature for 200 ps. This difference in cooling rate provided during the processing of BMG may have significant effects on the structural and mechanical behavior of the sample configuration. To study the mechanical behavior, nanoindentation technique is utilized. A spherical rigid Cu indenter (diameter = 60 Å) is used to indent the sample at a constant velocity of 10 m/s. The resulting load-depth and hardness-depth curves for different cooling rates are compared as shown in Figs. 6 and 7 respectively.

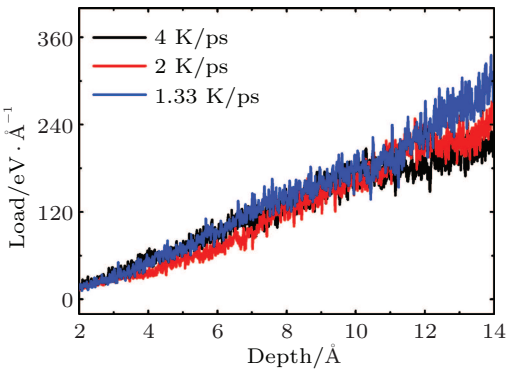

Fig. 6. (color online) Plots of load versus depth, showing the effects of different cooling rates.

The load-depth curves for three samples reveal that the load for the lowest cooling rate is higher than that for higher cooling rates. Similarly, hardness-depth curves also reveal that sample with the least cooling rate is hardest in all the samples and vice versa. This effect is due to the certain structural variations during the processing of BMGs at different cooling rates. To describe the possible difference in the final structure, the curves of RDF versus interatomic distance are compared as shown in Fig. 8.

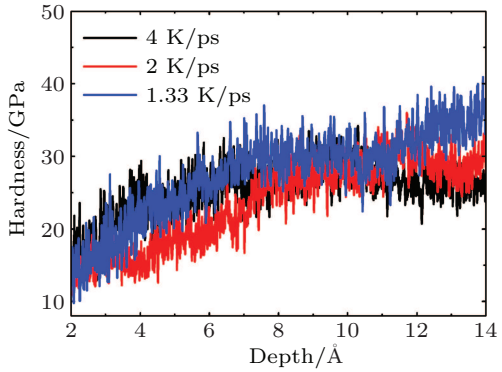

Fig. 7. (color online) Plots of hardness versus depth, indicating the effects of different cooling rates.

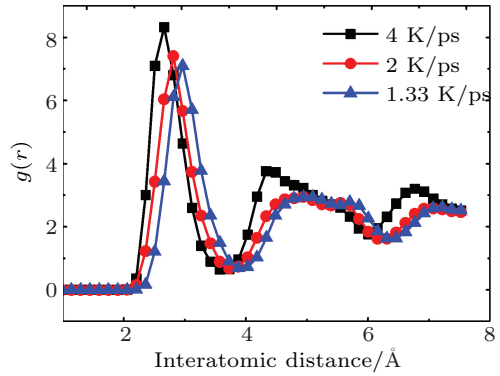

Fig. 8. (color online) Plots of RDF versus interatomic distance, exhibiting the effects of different cooling rates.

Figure 8 shows clearly the difference in final structural configuration among all three samples. The first peak is high for higher cooling rate compared with those of the samples cooled at slow cooling rates. This indicates that that sample with a slow cooling rate is more stable than the abruptly quenched sample. Hence, it can be noted that the sample with the highest cooling rate appears to be less hard than the slowly cooled samples. Earlier studies showed that serrated flow during the indentation induced deformation is highly sensitive to the processing technique (cooling rate) of BMG. This can also be one of the important factors affecting the mechanical behavior of the BMG. Results are similar to those provided in Refs. [39] and [40]. The deformation mechanism in BMG is entirely different from those in metals and alloys. We[43,44] studied previously that the deformation during the indentation in crystalline material mainly occurs through slipping of the crystallographic planes and movement of dislocations. However, BMG does not deform through the slipping and dislocation mechanism because of its amorphous structure. Serrated flow is known to be the basic deformation mechanism in BMG. The deformation behavior of $Cu_{50}Zr_{50}$ BMG under a spherical indenter is shown in Fig. 9.

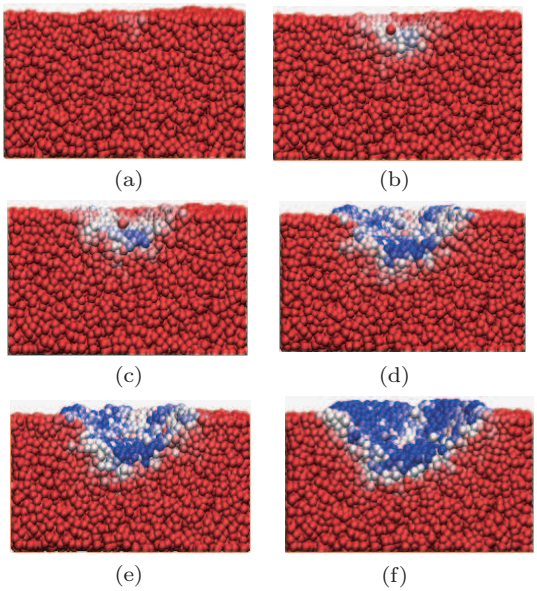

Fig. 9. (color online) Step-by-step (in (a)-to-(f) sequence) deformation of $Cu_{50}Zr_{50}$ BMG sample in the nanoindentation process. Half of the substrate atoms are removed while taking these snapshots for clear visualization of atomic deformation.

To highlight the atomic movement during the indentation process (in Fig. 9), the value of net displacement covered by each substrate is calculated using the following equation:

$$\text{Total displacement} = \sqrt{(\mathrm{d}x)^2 + (\mathrm{d}y)^2 + (\mathrm{d}z)^2}. \quad (1)$$

The atoms of the substrate are colored on the basis of total displacement covered by each atom (during deformation caused by indentation process). The deformation behavior of BMG substrate is clear from this figure. The deformed atoms change color on the basis of their total displacement. Hence, the stress concentration can be easily visualized under the indenter.

6. Conclusions

The present work is done to elucidate the mechanical behaviors of BMGs (different Cu and Zr based compositions by %). We perform the nanoindentations at three samples with different Cu and Zr concentrations ($Cu_{75}Zr_{25}$, $Cu_{50}Zr_{50}$, and $Cu_{25}Zr_{75}$) processed to form BMG samples. It is observed from the results that the mechanical behavior strongly varies with the component concentration in BMG. Values of load and hardness are highest for $Cu_{75}Zr_{25}$ and lowest for $Cu_{25}Zr_{75}$;

whereas those for $Cu_{50}Zr_{50}$ fall in between. The variation in the mechanical behavior may be related to the possible structural variation. RDF curves shows that $Cu_{75}Zr_{25}$ is more stable and hence harder than other sample configurations. To show the significance of cooling rate provided during the processing, $Cu_{50}Zr_{50}$ BMG is chosen for nanoindentation. It is observed that the sample prepared with relatively high cooling rate appears to be softer than the others quenched relatively at slower rate. RDF curves indicate that the possible structural variations are caused by the difference in quenching rate. It can be concluded that BMG appears more stable and harder by making the quenching rate relatively slow.

Acknowledgment

This work was carried out in the Department of Physics Simulation Lab, the Islamia University of Bahawalpur.

References

[1] Johnson W L 2002 *J. Miner. Met. Mater. Soc.* **54** 40
[2] Jeong H W, Hata S and Shimokohbe A 2003 *J. Microelectromech. S.* **12** 42
[3] Sambandam S N, Bhansali S and Bhethanabotla V R 2004 *Mater. Res. Soc. Symp. Proc.* **806**
[4] Saotome Y, Noguchi Y, Zhang T and Inoue A 2004 *Mater. Sci. Eng. A* **389** 375
[5] Schuh C A, Hufnagel T C and Ramamurty U 2007 *Acta Mater.* **55** 4067
[6] Chen M 2008 *Rev. Mater. Res.* **38** 445
[7] Trexler M M and Thadhani N N 2010 *Prog. Mater. Sci.* **55** 759
[8] Dreham A L, Greer A L and Turnbull D 1982 *Appl. Phys. Lett.* **41** 716
[9] Inoue A, Zhang T and Masumoto T 1990 *Mater. Trans. JIM* **31** 425
[10] Zhang T, Inoue A and Masumoto T 1991 *Mater. Trans. JIM* **32** 1005
[11] Inoue A and Takeuchi A 2002 *Mater. Trans. JIM* **43** 1892
[12] Wang W H, Dong C and Shek C H 2004 *Mater. Sci. Eng. R* **44** 45
[13] Li Y, Guo Q, Kalb J A and Thompson C V 2008 *Science* **322** 1816
[14] Mattern N, Schops A, Kuhn U, Acker J, Khvostikova O and Eckert J 2008 *J. Non-Cryst. Solids* **354** 1054
[15] Mattern N, Jovari P, Kaban I, Gruner S, Elsner A, Kokotin V, Franz H, Beuneu B and Eckert J 2009 *J. Alloy. Compd.* **485** 163
[16] Mattern N, Bednarcik J, Pauly S, Wang G, Das J and Eckert 2009 *Acta Mater.* **57** 4133
[17] Antonowicz J, Pietnoczka A, Zalewski W, Bacewicz R, Stoica M, Georgarakis K and Yavari A R 2011 *J. Alloy. Compd.* **509S** S34
[18] Inoue A 2000 *Acta Mater.* **48** 279
[19] Wright A J, Saha R and Nix W D 2011 *Mater. Trans. JIM* **42** 642
[20] Kang B C, Kim H Y, Kwon O Y and Hong S H 2007 *Scr. Mater.* **57** 703
[21] Barshilia H C and Rajam K S 2002 *Surf. Coat. Technol.* **195** 155
[22] Chudoba T, Schwarzer N, Richter F and Beck U 2000 *Thin Solid Films* **377** 366
[23] Oliver W C and Pharr G M 1992 *J. Mater. Res.* **7** 1564
[24] Hay J L and Pharr G M 2000 *ASM Handbook* (ASM International)
[25] Vaidyanathan R, Dao M, Ravichandran G and Suresh S 2001 *Acta Mater.* **49** 3781
[26] Schuh C A and Nieh T G 2004 *J. Mater. Res.* **19** 46
[27] Puthucode A, Banerrjee R, Vadlakonda S, Mirshams R and Kaufman M J 2008 *Metall. Mater. Trans. A* **39** 1552
[28] Bei H, Lu Z P and George E 2004 *Phys. Rev. Lett.* **93** 125504
[29] Liu L and Chan K C 2005 *Mater. Lett.* **59** 3090
[30] Lagogianni A E, Almyras G, Lekka C E, Papageorgiou D G and Evangelakis G A 2009 *J. Alloy. Compd.* **483** 658
[31] Pang J J, Tan M J, Liew K M and Shear W C 2012 *Physica B* **40 7** 340
[32] Raghavan R, Kombaiah B, Dobeli M, Erni R, Ramamurty U and Michler J 2012 *Mate. Sci. Eng. A* **532** 407
[33] Yoo B G, Oh J H, Kim Y J, Park K W, Lee J C and Jang J I 2010 *Intermetallics* **18** 1898
[34] Zhao L, Ma C L, Fu M W and Zeng X R 2012 *Intermetallics* **30** 65
[35] Wang J, Hodgson P D, Zhang J, Yan W and Yang C 2010 *Comp. Mater. Sci.* **50** 211
[36] Shi Y and Falk M L 2007 *Thin Solid Films* **515** 3179
[37] Deng S C and Christopher A 2012 *Appl. Phys. Lett.* **100** 251909
[38] Duraru A P, Andersen U G, Thyssen A, Bailey N P, Jacobsen K W and Schiøtz J 2010 *Modelling Simul. Mater. Sci. Eng.* **18** 055006
[39] Shi Y and Falk M L 2007 *Acta Mater.* **55** 4317
[40] Shi Y and Falk M L 2006 *Scripta Mater.* **54** 381
[41] Finnis M W and Sinclair I E 2007 *Phil. Mag. A* **50** 45
[42] Plimpton S J 1995 *J. Comput. Phys.* **117** 1
[43] Imran M, Hussain F, Rashid M and Ahmad S A 2012 *Chin. Phys. B* **21** 126802
[44] Imran M, Hussain F, Rashid M and Ahmad S A 2012 *Chin. Phys. B* **21** 116201